Assembly of Colloidal Molecules, Polymers, and Crystals in Acoustic and Magnetic Fields

Ye Yang, An T. Pham, Daniela Cruz, Christopher Reyes, Benjamin J. Wiley, Gabriel P. Lopez, and Benjamin B. Yellen**

Naturally occurring materials are formed from the self-assembly of atoms into myriad of constructs, such as molecules,[1–3] cross-linked networks,[4–6] amorphous glasses, and crystalline solids.[7,8] The vast atomic permutations and structural variations of these materials leads to diverse mechanical, thermal, electromagnetic, and chemical properties, which can be tuned for human benefit. Drawing inspiration from nature's "bottom up" self-assembly principles,[9,10] materials scientists are developing large-scale, low-cost synthesis paradigms that employs colloidal particles (i.e., as macro-atoms) to synthesize functional materials.[11–16] The ability to mimic the different length scales and arrangements of natural materials, ranging from small molecules[17–19] to polymers chains/networks[20–22] and glasses/crystals[23–26] has various engineering applications,[11,12] ranging from photonic[27–29] and phononic[30,31] waveguides to self-assembled battery electrodes.[32,33] However, most colloidal interactions tend to be isotropic, which limits the diversity of achievable structures, whereas atoms display highly directional bonding and can form into a broader class of structures.

The quest to increase the diversity of colloidal assemblies has spurred several branches of research. One branch focuses on the synthesis of anisotropic particles, such as Janus[24,34] and patchy particles,[17] which can reproduce the directional bonding features of atomic scale interactions. However, unlike spherically symmetric particles, these engineered particles are limited to small-scale production. A second branch focuses on colloidal alloys (e.g., two or more particle types mixed at different ratios), which have been assembled by controlling the kinetics of drying films,[16] or by adjusting the charge or dipole moments of the particles.[19,26] Unlike single component systems, colloidal alloys have slow equilibration times and high defect rates, which limits potential applications. A third branch focuses on colloidal assembles in a combination of vertical confinement and multi-field interactions, including recent work on magnetic and optical fields,[35] and electrohydrodynamics (EHD)/dielectrophoresis (DEP).[18,36] These multi-field confinement approaches can use spherical colloidal particles, which can be synthesized with high monodispersity and in large quantities, and thus offer more opportunity for large-scale production.

The assembly of colloidal structures in external driving fields has been widely explored due to the convenient ability to adjust the strength of particle interactions *in situ*, and thereby mimic an effective system temperature. An effective system pressure can also be emulated to control the local particle concentration, either with local field gradients or with external fluid flows. However, there has been significantly less work on developing techniques to simultaneously control the equivalent temperature and pressure in colloidal systems, which would allow the phase space to be more efficiently explored. Currently existing approaches either have small dynamic range,[18,35] or employ strongly correlated fields that are not independently controllable,[36] which limits utility and reduces the diversity of the resulting assemblies.

We report a new assembly technique that solves the above issues by using multiple fields to drive the assembly – an acoustic standing wave is used to control the particle concentration, and a uniform external magnetic field is used to control the interparticle interactions. We show the ability to assemble a large class of structures, ranging from discrete colloidal molecules and polymer networks, to well-ordered crystals, by tuning the ratio of the magnetic and acoustic field strengths and their magnitudes relative to gravity and surface adhesion forces. The magnetic field induces dipole–dipole interactions, which is tunable with the magnetic field strength and plays a role similar to controlling the effective temperature of the suspension: $T^* = 144 k_B T / \pi \mu_0 \sigma^3 \overline{\chi}^2 H^2$, where σ, μ_0, k_B, T, $\overline{\chi}$, and H are the particle diameter, vacuum permeability, Boltzmann constant, real temperature, shape-corrected magnetic susceptibility, and the field strength, respectively. The acoustic field controls the local density of particles by attracting them to the pressure nodes of the standing wave, and thereby plays a role similar to

Y. Yang, A. T. Pham, G. P. Lopez, B. B. Yellen
Department of Mechanical Engineering
and Materials Science
Duke University
Box 90300 Hudson Hall, Durham, NC 27708, USA
E-mail: gabriel.lopez@duke.edu; yellen@duke.edu
Y. Yang, A. T. Pham, D. Cruz, C. Reyes, B. J. Wiley,
G. P. Lopez, B. B. Yellen
NSF Research Triangle Materials Research
Science and Engineering Center (MRSEC)
Duke University
Box 90217, Durham, NC 27708, USA
D. Cruz, G. P. Lopez, B. B. Yellen
Department of Biomedical Engineering
Duke University
Durham, NC 27708, USA
C. Reyes, B. J. Wiley
Department of Chemistry
Duke University
Durham, NC 27708, USA
B. B. Yellen
University of Michigan – Shanghai Jiao Tong University
Joint Institute, Shanghai Jiao Tong University
800 Dong Chuan Rd, Shanghai 200240, China

DOI: 10.1002/adma.201500462

ADVANCED MATERIALS
www.advmat.de

www.MaterialsViews.com

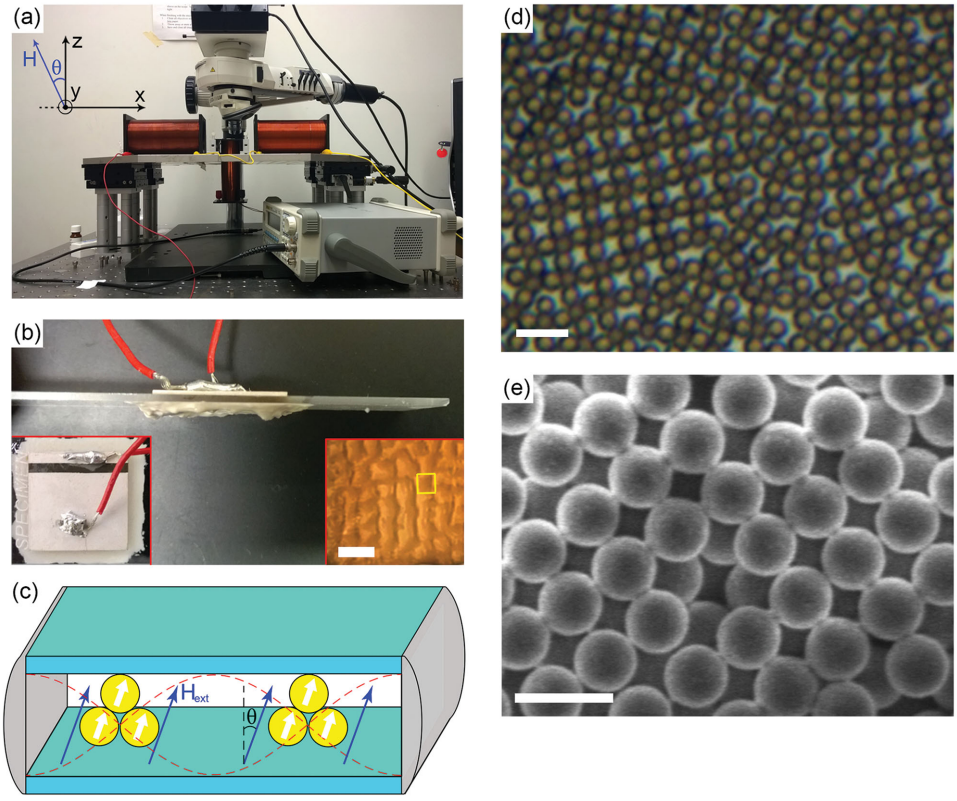

Figure 1. Experimental system overview. The experimental system shown in (a) includes a pair of horizontal coils and a vertical coil mounted underneath the sample to generate a bi-axial magnetic field. A piezoelectric transducer (PZT) mounted on the sample exterior (b) is driven by a signal generator to create the acoustic standing wave pattern, attracting particles into an array of nodes shown in the right inset of (b). The side and back images (left inset) show how the transducer was mounted, and the yellow rectangle indicates the region of interest in a typical experiment. c) A side-view illustration of the experimental apparatus, showing that the particles are attracted to the pressure node of the acoustic standing wave (not drawn to scale). d) An assembled bilayer of non-close-packed tetragonal lattice. e) A SEM image of a bilayer body-centered-tetragonal (BCT) structure after photoacid-induced stabilization and drying. The scale bars are 2.5 mm for the right inset in (b), (d) 10 μm and (e) 5 μm, respectively.

controlling the local pressure of the suspension. By simultaneously controlling these two fields, a wide range of phase space can be explored in a single experiment.

Figure 1 provides an overview of the experimental system. The sample consists of a thin fluid film containing a suspension of superparamagnetic particles sealed between a glass slide and coverslip. The fluid film thickness is tuned to be slightly larger than the particle diameter. Vertical and horizontal coils arranged around the sample produce a bi-axial magnetic field, in which the tilt angle, θ, can be controlled relative to the vertical direction (Figure 1a). The PZT transducer element mounted on the glass slide (Figure 1b) induces an acoustic standing wave in the fluid chamber when excited by a signal generator, causing the particles to concentrate into an array of pressure nodes (see the right inset of Figure 1b). In this work, the PZT transducer is excited at 2.932 MHz, which corresponds to an acoustic wavelength of ca. 500 μm. The regions of high particle concentration have a characteristic length of ca. 100–200 μm, which limits the grain size for these experimental conditions. It is possible to increase the grain size by increasing the acoustic wavelength. Figure 1c provides an illustration of particles in the pressure node and exposed to a uniform magnetic field inside a vertically confined fluid film. If the sample contains either initially high particle concentration or the PZT is excited at high driving amplitudes, the particles assemble into networks or crystal structures near the center of the pressure nodes (Figure 1d). Once the desired structures have been assembled, they can be stabilized by exciting a dissolved photoacid generator, which lowers the suspension pH and causes the particles to bind irreversibly rendering the structures stable upon drying. See the scanning electron microscopy (SEM) image of Figure 1d.

Vertical confinement plays a critical role in determining the types of structures formed. In perfectly 2D confined systems, the dipole–dipole interactions between magnetic particles are isotropic and purely repulsive in a vertical field, expressed as $U_{ij} = (\mu_f m_i m_j) / 4\pi r_{ij}^3$ (see the Supporting Information for details). As a result, the only stable phase is a hexagonal lattice of particles. On the other hand, when the particles are allowed to buckle by a small amount in the vertical direction, the magnetic interactions become anisotropic, leading to new structures of various types, which are adjustable with the film thickness and the local particle concentration (**Figure 2**).

In order to better understand the experimental system, we calculated the potential energy of clusters of interacting magnetic point dipoles, which are plotted as a function of the volume fraction (η), shown in Figure 2h. Due to the low magnetic fields employed, we found that gravitational and surface

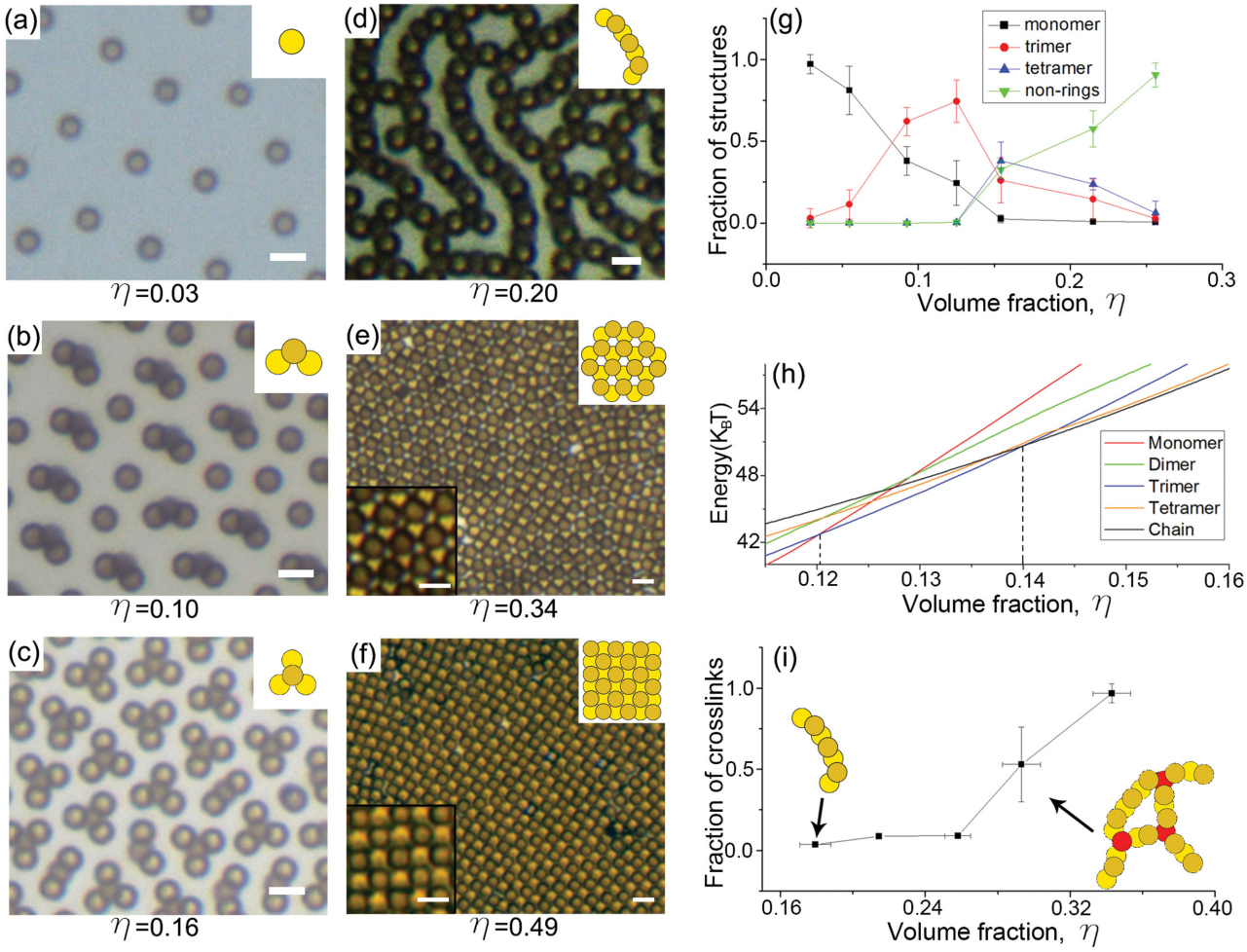

Figure 2. Colloidal structures in a vertical magnetic field. In a vertical external magnetic field of $H = 6$ Oe ($T^* = 0.0682$), we tuned the colloidal structures by modulating the acoustic driving input, which controls the local particle concentration. At different concentrations, η, we were able to form a) monomers for $\eta = 0.03$, b) trimers for $\eta = 0.10$, c) tetramers for $\eta = 0.16$, d) chains for $\eta = 0.20$, e) n-HCP lattice for $\eta = 0.34$, and f) bilayer BCT lattice for $\eta = 0.49$. Illustrations of each of the structures are provided in the top-right insets, and high magnification images are provided in the bottom-left inset for (e) the n-HCP lattice and (f) the BCT lattice. In (g), we report the relative number fraction of particles forming discrete structures (e.g., monomers, dimers, trimers, tetramers, and short chains). Experiments agree reasonably well with analytical predictions (h), which shows the potential energy of each structure as a function of concentration. At higher local concentrations, we quantified the fraction of cross-linked particles in (i) within colloidal polymer networks. The red particles in the illustration represent a "crosslinked particle," and yellow particles represent "non-crosslinked" particles. The scale bars are 5 μm in (a)–(f).

adhesion interactions were non-negligible, and their inclusion markedly improved the agreement with experiment (see the Supporting Information for details). At low particle concentrations, a hexagonal array of isolated particles (monomers) minimizes the system potential energy. Discrete particle clusters, here referred to as bent trimers and tetramers (Figure 2b,c), that are reminiscent in structure to H_2O and NH_3 molecules, were observed once the local concentration exceeds critical thresholds of $\eta = 0.09$ and $\eta = 0.15$, respectively. In weak vertical magnetic field $H = 6$ Oe ($T^* = 0.0682$) our potential energy calculations indicate that bent trimers were the minimum energy state for concentrations in the range of $\eta = 0.12$–0.14. In strong vertical field of $H > 12$ Oe ($T^* < 0.0170$), on the other hand, the dimer structure was the minimum energy configuration, due to the increased relative importance of the magnetic interaction (see the Supporting Information for more details).

At higher concentrations, we observe zigzag structures with bond angles of nearly 120° that are reminiscent of carbon chains in alkyl compounds. As the concentration increases further, these chains polymerize into percolated networks (Figure 2d). Chain structures become minimum energy configurations at volume fractions of $\eta > 0.14$. We note that for $0.14 < \eta < 0.16$, the potential energy difference between the tetramers and chains is small, which explains why these structures frequently coexisted. When $\eta > 0.16$, the chain structures and networks became the sole minimal energy state.[36] As the particle concentration increases further to $\eta > 0.35$, the lamellar phase of loosely connected chains is compacted into several types of bilayer crystal structures, including both close-packed and non-close-packed hexagonal (n-HCP) structures, as well as body-centered-tetragonal (BCT) structures. The n-HCP and BCT lattices are shown in Figure 2e,f, respectively. An example

of the transformation from n-HCP to BCT lattice when the acoustic field is increased is provided in Movie S1, Supporting Information.

In our experiments, the fluid cell thickness was estimated to be h = 1.4σ, where σ is the particle diameter. This estimate comes from particle size and interparticle separation distance measurements obtained with ImagePro. To characterize the formation of discrete particle clusters, we measured the relative number of each cluster type in the particle concentration regime of $\eta \leq 0.18$, shown in Figure 2h. Colloidal monomers were predominantly observed for $\eta \leq 0.05$. The relative fraction of trimers to monomers gradually increases as η approaches 0.12. As η was further increased to 0.16, the relative fraction of monomers/trimers decreased, and the chains/tetramers increased. For $\eta \geq 0.16$, chain structures were the dominant phase. These results correspond qualitatively well with the minimum energy plots of Figure 2h, which show that monomers have the lowest energy when $\eta < 0.12$, trimers have the lowest energy when $0.12 \leq \eta < 0.14$, tetramers and chains have similar energy when $0.14 \leq \eta < 0.16$, and finally chain phases have the lowest energy state when $\eta \geq 0.16$. There are two other important control parameters, namely, the strength of the magnetic field, and the degree of vertical confinement. In these experiments, the magnetic field was kept fixed at $H = 6$ Oe ($T^* = 0.0682$), which provided sufficient particle–particle interactions to maintain the assemblies against thermal fluctuation, while still allowing the system to efficiently reach equilibrium. The effect of tuning the magnetic field strength was found to be consistent in experiments and in molecular dynamics simulations (Figure S4, Supporting Information). The vertical confinement was also found to play a role in the assembled morphology in simulation; however the variation in the assembled structures were relatively minor when the thickness of the fluid layer was maintained in the range of 1.3–1.7 particle diameters.

To characterize the polymerization of chains into percolated networks, we measured the crosslink density of the chain structures in the regime $\eta \geq 0.18$, shown in Figure 2i. The crosslink density is defined as the percentage of particles that are in direct contact with at least 3 other particles, e.g., the red particles in the illustration of Figure 2i. This definition simplifies the description of the transformation from polymer to crystal phases: When a particle is in direct connection with at least three other particles, it will act as a crosslink node, and in a crystalline phase, every particle is crosslinked regardless of the specific number of bonds in that crystal arrangement. For $0.16 < \eta < 0.18$, the crosslinking density is small and the system consists primarily of a mixture of short polymer chains. For $\eta \geq 0.34$, the crosslink density approaches unity, and the particle pack into a non-close-packed hexagonal crystal (n-HCP), shown in Figure 2e. As η is further increased, the particles will be further packed together into crystal phase, and form a BCT lattice, shown in Figure 2f.

Next, we analyzed structures formed in a tilted magnetic field, which has analogies at the molecular scale with electric field induced orientation of discrete molecules and polymer chains. Previous experiments[37,38] and simulations[39] have demonstrated interesting anisotropic phases in bi-axial electric fields, and similar studies have been performed in magnetic systems.[40,41] However, bi-axial field techniques cannot independently control the local particle concentration, and thus they produce a different set of structures compared to those reported here. Moreover, prior investigations did not explore the effects of confinement. Characteristic examples of the assemblies are shown in **Figure 3**, in which the rows depict the assemblies at tilt angles of $\theta = 0°$, 25°, 45°, 65°, and 90°, and the columns represent the assemblies in volume fractions of $\eta \approx 0.10$, $\eta \approx 0.24$, and $\eta \approx 0.46$. At low particle concentration (Figure 3, 1st column), the particles form a distribution of monomers, dimers, and bent trimers. In the vertical field, the bent trimers have random orientations (Figure 3a); however when the tilt angle is increased from $25° < \theta < 45°$, the bent trimers become aligned with the in-plane field component. We also begin to observe linear trimers, which stretch along the in-plane field direction. The linear structures dominate when $\theta > 60°$, and culminate in the formation of extended linear chains.

For intermediate particle concentrations (Figure 3, 2nd column), there is a striking interplay between the chain direction and the bond angles within the chain. As the tilt angle is increased from $\theta = 0°$ to 90°, the chain direction first becomes oriented perpendicular to the in-plane field component (Figure 3g, $\theta = 25°$). At higher tilt angles, the chain direction becomes increasingly aligned with the external field direction, whereas the bond angles in the chain decrease (Figure 3h,i). The behavior of assembled structures is very different at high concentration of $\eta \approx 0.46$, in which the particles form multi-domain BCT and HCP crystals irrespective of the field direction.

To better characterize this structural dependence, we analyze the chain direction and the bond angle for bent trimers (**Figure 4**e) and zigzag chains (Figure 4f) as a function of the tilt angle, θ. For both the bent trimers and the zigzag chains, the bond angle (red data points) decreases from $\psi = 120°$ to $\psi \approx 60$–70° as the tilt angle is increased. In a vertical field, the bent trimers and chain directions initially have a random distribution(Figure 3a,f for $\theta = 0°$). As the tilt angle is increased, the chain direction of the bent trimers becomes increasingly aligned perpendicular to the in-plane field (Figure 3b and 4b). The orientation of chains is more complicated and involves multiple competing energies. As θ is increased, the chains first display perpendicular orientation near $\theta = 20°$ (Figure 3g and 4c), but this trend reverses and results in alignment with the in-plane field component for larger tilt angles near $\theta = 60°$. The different behaviors between trimers and chains arise from the stronger couplings between particles within the chain phases compared to the bent trimers.

The beauty of this experimental system is its ability to coax particles to form a desired structure prior to locking it in by chemical techniques. Here, we demonstrate proof-of-principle by immersing the magnetic particles in a solution of photoacid generator (0.1 M pyranine). In the presence of UV light, the photoacid generator lowers the solution pH, which tunes the surface charge density on the colloidal particles past the isoelectric point. The absence of a stabilizing electrostatic double layer thus causes the particles to condense into a primary van der Waals energy minimum,[42,43] which is stable even when the system returns to its original conditions or is dried. After one hour of UV exposure, the assembled structures were stable even after the fields are turned off. Some of the structures, including

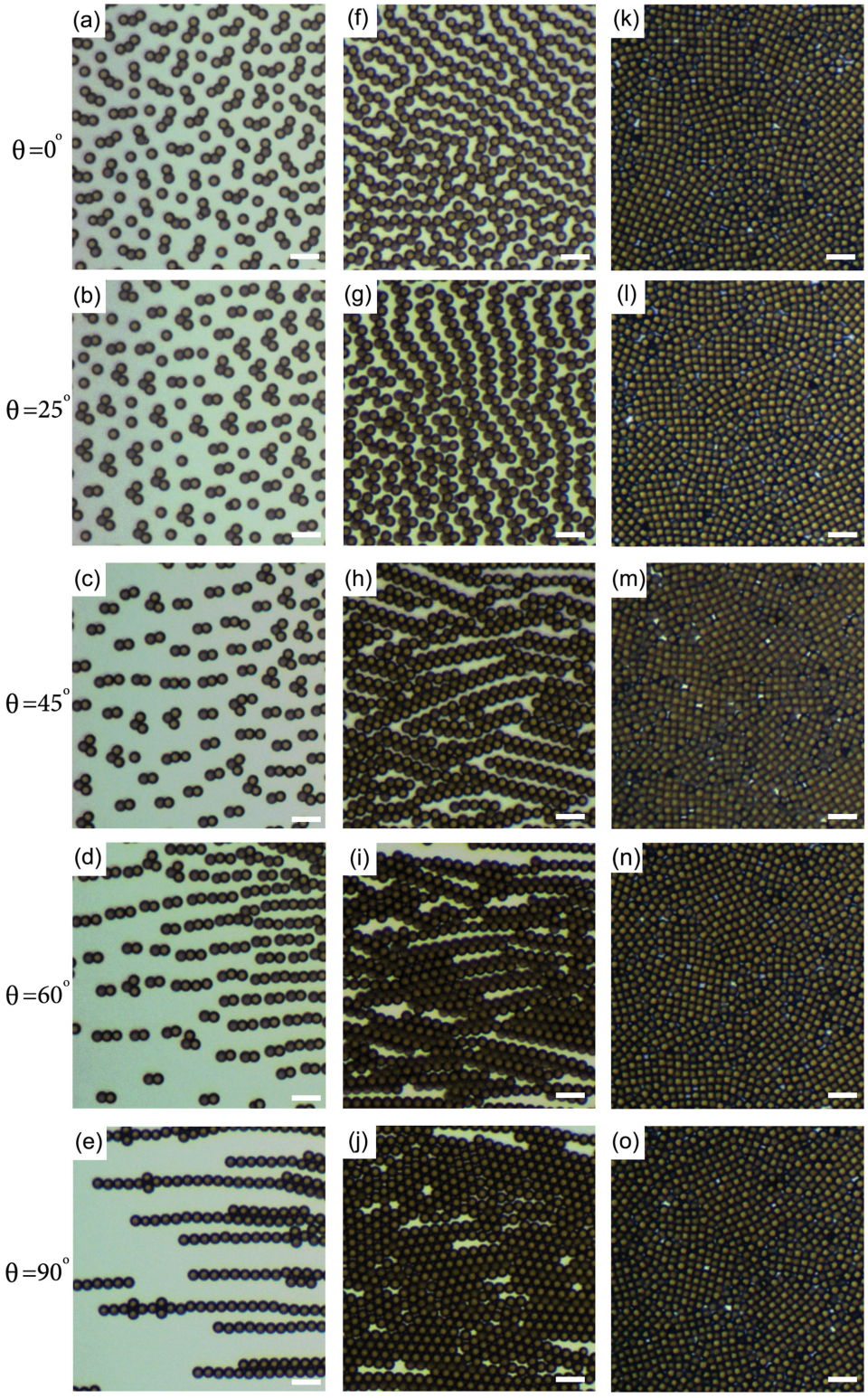

Figure 3. Colloidal structures in a tilted magnetic field. Each row depicts a constant magnetic field tilt angle, while each column depicts a constant local particle concentration, which was selected to form either: a–e) trimer structures for $\eta \approx 0.10$, f–j) chains structures for $\eta \approx 0.24$, or k–o) BCT lattice structures for $\eta \approx 0.46$. At small tilt angles of $\theta < 10°$, the trimer and chain alignments (a,f) are dramatically different from the alignments at intermediate tilt angle of $\theta \approx 25°$ (b,g) and at large tilt angles of $\theta > 45°$ (c,h). (c,d) The trimers transform into dimers and in-plane chains when θ is increased above 45°, and the chains transform into BCT or HCP crystallites when θ is increased above 60°. For high particle concentrations (k–o), the structures were unchanged regardless of the field direction. The scale bars are 10 μm.

ADVANCED MATERIALS
www.advmat.de

www.MaterialsViews.com

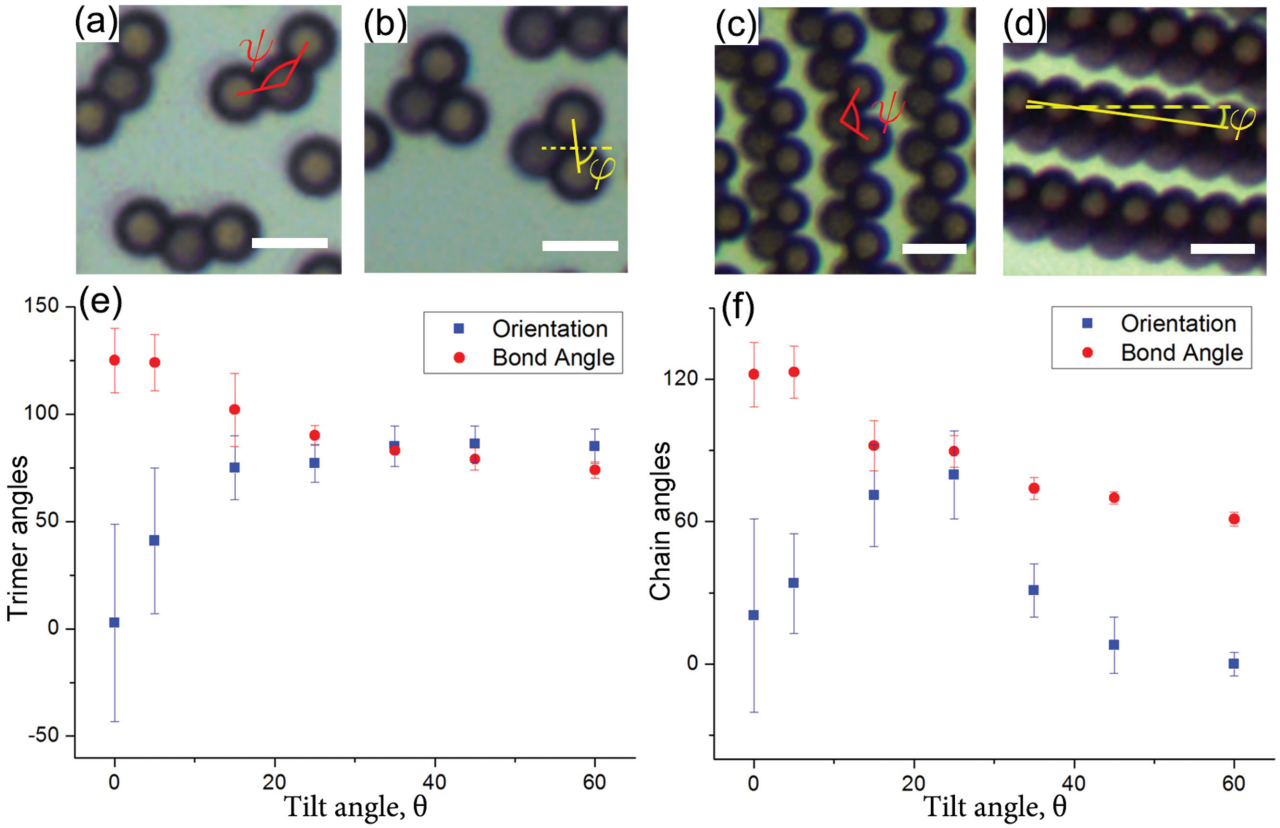

Figure 4. Bond angles and chain directions in a tilted magnetic field. The definition of the bond angles (ψ) and chain directions relative to the in-plane field component (φ) are illustrated in (a,b) for trimers, and (c,d) for chains. Measurements of the bond angles and chain directions with respect to tilt angle θ are presented in (e) for trimers, and (f) for chains. The measurements are performed on at least 20 different structures for each tilt angle. The large standard deviation in chain direction is indicative of the random orientation that occurs in a purely vertical magnetic field, whereas an applied horizontal field component leads to smaller standard deviations and corresponds to more uniformly aligned structures. The field strength is H = 6 Oe ($T^* = 0.0682$), in all the experiments. The particle concentration is $\eta \approx 0.1$ for bent trimers (a,b,e) and $\eta \approx 0.24$ for chains. The scale bars in all images are 5 μm.

dimers, trimers, chains, as well as BCT crystals were preserved after drying of the sample (Figure S6, Supporting Information, and Figure 1d), which indicates that this fixation method is sufficient to withstand the strong meniscus forces of drying processes. In principle, it should be possible to fix only the desired assemblies by applying selective photo-illumination, such as flood exposure through a photomask, or local sintering with a laser beam. We also note that once the conditions for assembling a desired structure is known, it is possible to directly control the suspension concentration without requiring an acoustic field. This approach would have the benefit of increasing the uniformity of the desired structures and thereby render this system more amenable to large-scale fabrication.

In conclusion, we present a novel magneto-acoustic assembly platform, which can adjust the type of assembled structure *in situ*, and therefore enable the formation of a large class of structures ranging from discrete clusters to well-ordered crystals. Here, we focus on micron-sized colloidal particles due to its convenience in tracking the structures in an optical microscope. However, in principle it is possible to scale this assembly technique well into the sub-micrometer regime, and it has already been demonstrated that magnetic[27] and acoustic interactions[44,45] can dominate over thermal energy even when the particle sizes are comparable to (or smaller than) optical wavelengths. The ability to stabilize the structures and transfer them to other substrates shows promise for future applications in biosensors and photonic devices.

Experimental Section

Materials: Experiments used 2.7 μm carboxylated magnetic particles (M-270 Dynabeads, Life Technologies). To prevent adhesion between the particles and the substrates, the glass slides and coverslips were functionalized with 10 kD silane–polyoxyethylene–carboxylic acid (PG2-CASL-10k, NANOCS, New York, NY, USA). For stabilization of colloidal structures, a type of photoacid, namely pyranine (Tokyo Chemical Industry, Japan) was used to replace water in the colloidal suspension before the assembly experiment.

Sample Preparation: The magnetic particles were concentrated to a volume fraction of 0.05 in the final suspension by centrifugation. An aliquot of colloidal suspension (1.9 μL) was inserted between a pair of glass slide and coverslip, and sealed with marine Epoxy (Loctite) to prevent convection and evaporation.

Magneto-Acoustic Assembly: The bi-axial magnetic fields were created by passing DC current to air core magnetic solenoids (Fisher Scientific, Pittsburgh, PA, USA). The currents were supplied by a bipolar operational power amplifier (KEPCO, Flushing, NY, USA) and controlled by LABVIEW (National Instruments, Austin, TX, USA). In the experiments of Figure 3,

the direction of the external field is tilted at a rate of 1° min^{-1}. The acoustic field was supplied by inputting a 2.93 MHz sinusoidal wave to a piezoelectric transducer (APC International, Mackeyville, PA, USA) using a function signal generator (Rigol, Beaverton, OR, USA).

Structure Stabilization: To stabilize the colloidal structures, the fluid was replaced with 0.1 M pyranine (Tokyo Chemical Industry, Japan). After the colloidal structures were tuned to the desired configuration, the sample was exposed to 365 nm UV light with a power density of ca. 36 mW cm^{-2} for 1.5 h in the presence of magnetic and acoustic field. Next, the sample was then taken out of the external field and heated to 120 °C for 2 h. The coverslip was then carefully removed from the sample, and the residual structures on the glass slide were dried in air for SEM imaging (Figure S6, Supporting Information).

Simulations and Analytical Calculations: Details of the theory and analytical calculation methods are included in the Supporting Information.

Supporting Information

Supporting Information is available from the Wiley Online Library or from the author.

Acknowledgements

The authors gratefully acknowledge support from the National Science Foundation through the Research Triangle MRSEC (DMR-1121107) and support from National Natural Science Foundation of China (NSFC-51350110334) and the China Youth 1000 Scholars Program.

Received: January 28, 2015
Revised: April 2, 2015
Published online: July 14, 2015

[1] G. C. Maitland, M. Rigby, E. B. Smith, W. A. Wakeham, *Intermolecular Forces: Their Origin and Determination*, Clarendon Press, Oxford, UK **1981**.
[2] L. M. Adleman, *Toward a Mathematical Theory of Self-Assembly*, Technical Report, Department of Computer Science, University of South California, CA, USA **1999**.
[3] E. Lifshitz, L. Pitaevskii, *Statistical Physics, Landau and Lifshitz Course of Theoretical Physics, Vol 9*, Butterworth-Heinemann, Oxford, UK **1980**.
[4] W. H. Carothers, *J. Am. Chem. Soc.* **1929**, *51*, 2548
[5] R. J. Cohen, G. B. Benedek, *J. Phys. Chem.* **1982**, *86*, 3696.
[6] M. Wertheim, *J. Chem. Phys.* **1987**, *87*, 7323.
[7] R. P. Andres, J. D. Bielefeld, J. I. Henderson, D. B. Janes, V. R. Kolagunta, C. P. Kubiak, W. J. Mahoney, R. G. Osifchin, *Science* **1996**, *273*, 1690.
[8] D. Turnbull, M. H. Cohen, *J. Chem. Phys.* **1961**, *34*, 120.
[9] G. M. Whitesides, B. Grzybowski, *Science* **2002**, *295*, 2418.
[10] G. M. Whitesides, J. P. Mathias, C. T. Seto, *Science* **1991**, *254*, 1312.
[11] M. Shimomura, T. Sawadaishi, *Curr. Opin. Colloid Interface Sci.* **2001**, *6*, 11.
[12] W. Lu, C. M. Lieber, *Nat. Mater.* **2007**, *6*, 841.
[13] F. Li, D. P. Josephson, A. Stein, *Angew. Chem. Int. Ed.* **2011**, *50*, 360.
[14] W. M. Choi, O. O. Park, *Nanotechnology* **2006**, *17*, 325.
[15] O. D. Velev, A. M. Lenhoff, *Curr. Opin. Colloid Interface Sci.* **2000**, *5*, 56.
[16] Y. Xia, Y. Yin, Y. Lu, J. McLellan, *Adv. Funct. Mater.* **2003**, *13*, 907.
[17] Y. Wang, Y. Wang, D. R. Breed, V. N. Manoharan, L. Feng, A. D. Hollingsworth, M. Weck, D. J. Pine, *Nature* **2012**, *491*, 51.
[18] F. Ma, D. T. Wu, N. Wu, *J. Am. Chem. Soc.* **2013**, *135*, 7839.
[19] R. M. Erb, H. S. Son, B. Samanta, V. M. Rotello, B. B. Yellen, *Nature* **2009**, *457*, 999.
[20] O. D. Velev, K. H. Bhatt, *Soft Matter* **2006**, *2*, 738.
[21] H. R. Vutukuri, A. F. Demirörs, B. Peng, P. D. J. van Oostrum, A. Imhof, A. van Blaaderen, *Angew. Chem. Int. Ed.* **2012**, *124*, 11411.
[22] A. K. Agarwal, A. Yethiraj, *Phys. Rev. Lett.* **2009**, *102*, 198301.
[23] M. E. Leunissen, C. G. Christova, A. P. Hynninen, C. P. Royall, A. I. Campbell, A. Imhof, M. Dijkstra, R. van Roij, A. van Blaaderen, *Nature* **2005**, *437*, 235.
[24] Q. Chen, S. C. Bae, S. Granick, *Nature* **2011**, *469*, 381.
[25] E. R. Weeks, J. C. Crocker, A. C. Levitt, A. Schofield, D. A. Weitz, *Science* **2000**, *287*, 627.
[26] A. Yethiraj, A. van Blaaderen, *Nature* **2003**, *421*, 513.
[27] J. Ge, Y. Hu, Y. Yin, *Angew. Chem. Int. Ed.* **2007**, *119*, 7572.
[28] A. Rogach, N. Kotov, D. Koktysh, J. Ostrander, G. Ragoisha, *Chem. Mater.* **2000**, *12*, 2721.
[29] P. V. Braun, R. W. Zehner, C. A. White, M. K. Weldon, C. Kloc, S. S. Patel, P. Wiltzius, *Adv. Mater.* **2001**, *13*, 721.
[30] M. Caleap, B. W. Drinkwater, *Proc. Natl. Acad. Sci. USA* **2014**, *111*, 6226.
[31] W. Cheng, J. Wang, U. Jonas, G. Fytas, N. Stefanou, *Nat. Mater.* **2006**, *5*, 830.
[32] H. Zhang, X. Yu, P. V. Braun, *Nat. Nanotechnol.* **2011**, *6*, 277.
[33] H. Yan, S. Sokolov, J. C. Lytle, A. Stein, Fan Zhang, W. H. Smyrl, *J. Electrochem. Soc.* **2003**, *150*, A1102.
[34] B. J. Park, T. Brugarolas, D. Lee, *Soft Matter* **2011**, *7*, 6413.
[35] N. Osterman, D. Babič, I. Poberaj, J. Dobnikar, P. Ziherl, *Phys. Rev. Lett.* **2007**, *99*, 248301.
[36] W. D. Ristenpart, I. A. Aksay, D. A. Saville, *Phys. Rev. Lett.* **2003**, *90*, 128303.
[37] M. Seul, D. Andelman, *Science* **1995**, *267*, 476.
[38] M. E. Leunissen, H. R. Vutukuri, A. van Blaaderen, *Adv. Mater.* **2009**, *21*, 3116.
[39] F. Smallenburg, M. Dijkstra, *J. Chem. Phys.* **2010**, *132*, 204508
[40] K. Müller, N. Osterman, D. Babič, C. N. Likos, J. Dobnikar, J. A. Nikoubashman, *Langmuir* **2014**, *30*, 5088.
[41] J. Dobnikar, A. Snezhko, A. Yethiraj, *Soft Matter* **2013**, *9*, 3693.
[42] V. Yadav, H. Zhang, R. Pavlick, A. Sen, *J. Am. Chem. Soc.* **2012**, *134*, 15688.
[43] R. J. Murphy, D. Pristinski, K. Migler, J. F. Douglas, V. M. Prabhub, *J. Chem. Phys.* **2010**, *132*, 194903.
[44] Y. Chen, X. Ding, S. Lin, S. Yang, P. Huang, N. Nama, Y. Zhao, A. Nawaz,F. Guo, W. Wang, Y. Gu, T. E. Mallouk, J. Huang, *ACS Nano* **2013**, *7*, 3306.
[45] C. Shields, D. Sun, K. A. Johnson, K. A. Duval, A. V. Rodriguez, L. Gao, P. A. Dayton, G. P. López, *Angew. Chem. Int. Ed.* **2014**, *53*, 8070.